

Online Bayesian Learning of Agent Behavior in Differential Games

Francesco Bianchin, Robert Lefringhausen, Sandra Hirche

*School of Computation, Information and Technology
(e-mail: {francesco.bianchin, robert.lefringhausen,
sandra.hirche}@tum.de}).*

Abstract: This work introduces an online Bayesian game-theoretic method for behavior identification in multi-agent dynamical systems. By casting Hamilton–Jacobi–Bellman optimality conditions as linear-in-parameter residuals, the method enables fast sequential Bayesian updates, uncertainty-aware inference, and robust prediction from limited, noisy data—without history stacks. The approach accommodates nonlinear dynamics and nonquadratic value functions through basis expansions, providing flexible models. Experiments, including linear–quadratic and nonlinear shared-control scenarios, demonstrate accurate prediction with quantified uncertainty, highlighting the method’s relevance for adaptive interaction and real-time decision making.

Keywords: Differential or dynamic games, Probabilistic and Bayesian methods for system identification, Learning methods for control, Multi-agent systems, Human–robot interaction

1. INTRODUCTION

In multi-agent settings, effective interaction increasingly depends on the ability to infer, predict, and adapt to the objectives of other agents. Collaborative, competitive, and mixed-autonomy scenarios—ranging from shared-control settings to multi-agent coordination and broader human–robot interaction—can all be modeled as differential games, in which each agent optimizes its own objective while interacting within a shared dynamical environment. Game-theoretic models provide a principled framework for describing such interactions (Isaacs, 1965; Basar and Olsder, 1999), and have proven effective for generating adaptive and anticipatory strategies across a variety of domains (Musić and Hirche, 2020; Li et al., 2016; Na and Cole, 2019).

A central challenge is that agent objectives are often unknown or only partially specified. Controllers that assume perfect knowledge of these objectives can perform poorly when agents deviate from the expected behavior, leading to degraded performance or unsafe outcomes. As a result, many practical approaches avoid constructing explicit models of human intent, opting instead for adaptive or heuristic strategies that respond to observed behavior (Li et al., 2016; Musić and Hirche, 2020). While successful in specific settings, these methods provide limited interpretability and lack robustness under irregular or hard-to-model behaviors.

Inverse Optimal Control (Self et al., 2021) and Inverse Reinforcement Learning (Arora and Doshi, 2021) aim to recover underlying objective functions from observations, offering structured models of decision making. Extensions to multi-agent settings via inverse differential games enable identification of individual objectives in coupled systems (Inga et al., 2021; Molloy et al., 2022). However, key chal-

lenges remain. Updates must be fast enough for online use (Self et al., 2021; Inga et al., 2021); moreover, real-world applications frequently involve nonlinear dynamics and nonquadratic value functions, extending beyond classical linear–quadratic (LQ) formulations (Engwerda, 2005; Inga et al., 2019; Bianchin et al., 2025). The general setting has been handled in different works by expressing the Hamilton–Jacobi–Bellman (HJB) optimality conditions underlying demonstrations as linear-in-parameter residuals, but existing methods either require extensive information on the agents’ objectives (Vamvoudakis and Lewis, 2011)—incompatible with settings involving unknown agents—or focus solely on single-agent problems (Self et al., 2018). Most importantly, inference must be robust to disturbances and behavioral variability. For example, human behavior routinely departs from nominal patterns, yet deterministic predictors cannot accommodate such deviations. Ensuring safety and reliability therefore requires uncertainty-aware inference that explicitly represents variability rather than assuming a single predicted trajectory. In addition, predictions should remain informative with limited initial data.

The main contribution of this paper is a Bayesian framework for inferring agent objectives in interactive settings from observed behavior. The method models approximate satisfaction of HJB optimality conditions and enables fast sequential updates through conjugate Gaussian inference, producing uncertainty-aware estimates of agent objectives at control frequencies. This formulation provides principled regularization through the formulation of priors, avoids the history-stack requirements common in prior approaches (Self et al., 2021), and yields informative predictions from limited data. The quantified uncertainty directly supports conservative or exploratory policies, enabling confidence-aware decision making in multi-agent interaction. The framework also extends naturally beyond

LQ assumptions: nonlinear dynamics and general value functions are accommodated via basis expansions, offering flexible yet interpretable models capable of capturing parametric and behavioral variation over time. We validate the approach in both LQ and nonlinear shared-control scenarios, demonstrating its practical relevance and applicability.

The remainder of the paper is structured as follows. Section II formulates the differential game model and the associated inverse problem. Section III introduces the approximate HJB regression framework. Section IV presents the online Bayesian estimator and its role in probabilistic prediction. Section V illustrates the approach in both linear-quadratic and nonlinear shared-control scenarios. Section VI concludes the paper.

2. PROBLEM FORMULATION

We consider a two-player, infinite-horizon, nonzero-sum differential game with dynamics

$$\dot{\mathbf{x}} = \mathbf{f}(\mathbf{x}) + \mathbf{g}_1(\mathbf{x}) \mathbf{u}_1 + \mathbf{g}_2(\mathbf{x}) \mathbf{u}_2, \quad (1)$$

where $\mathbf{x} \in \mathbb{R}^{n_x}$ and $\mathbf{u}_i \in \mathbb{R}^{n_{u_i}}$ denote the control inputs of players $i \in \{1, 2\}$. Each player minimizes the infinite-horizon cost

$$J_i(\mathbf{x}_0, \mathbf{u}_1, \mathbf{u}_2) = \int_0^\infty \left(Q_i(\mathbf{x}(t)) + \mathbf{u}_i(t)^\top \mathbf{R}_i \mathbf{u}_i(t) \right) dt, \quad (2)$$

where the state cost $Q_i : \mathbb{R}^{n_x} \rightarrow \mathbb{R}_{\geq 0}$ and the positive-definite matrix \mathbf{R}_i are unknown to the learner (which may be an external estimator or one of the players).

Remark 1. *The two-player setup is used for notational clarity; all definitions extend directly to N -player differential games with dynamics $\dot{\mathbf{x}} = \mathbf{f}(\mathbf{x}) + \sum_{i=1}^N \mathbf{g}_i(\mathbf{x}) \mathbf{u}_i$ and analogous cost functionals.*

We assume that the agents interact through stabilizing stationary feedback laws $\mathbf{u}_i = \boldsymbol{\mu}_i(\mathbf{x})$, yielding value functions

$$V_i(\mathbf{x}(t)) = \int_t^\infty \left(Q_i(\mathbf{x}(\tau)) + \boldsymbol{\mu}_i(\mathbf{x}(\tau))^\top \mathbf{R}_i \boldsymbol{\mu}_i(\mathbf{x}(\tau)) \right) d\tau. \quad (3)$$

We assume that the agents operate at a feedback Nash equilibrium (Basar and Olsder, 1999), namely a condition in which no component of the strategy pair $(\boldsymbol{\mu}_1^*, \boldsymbol{\mu}_2^*)$ can be changed unilaterally without increasing the corresponding player's cost. At any such equilibrium, (V_i, Q_i, \mathbf{R}_i) satisfy the coupled Hamilton–Jacobi–Bellman equations

$$0 = Q_i(\mathbf{x}) + \mathbf{u}_i^\top \mathbf{R}_i \mathbf{u}_i + \nabla V_i(\mathbf{x})^\top \left(\mathbf{f}(\mathbf{x}) + \mathbf{g}_1(\mathbf{x}) \mathbf{u}_1 + \mathbf{g}_2(\mathbf{x}) \mathbf{u}_2 \right) =: \mathcal{H}_i(\mathbf{x}, \mathbf{u}_1, \mathbf{u}_2), \quad (4)$$

and the stationarity of \mathcal{H}_i with respect to \mathbf{u}_i yields the equilibrium feedback law

$$\boldsymbol{\mu}_i^*(\mathbf{x}) = -\frac{1}{2} \mathbf{R}_i^{-1} \mathbf{g}_i(\mathbf{x})^\top \nabla V_i(\mathbf{x}), \quad (5)$$

which, by $\mathbf{R}_i \succ 0$, uniquely characterizes the optimal action for player i .

In the inverse setting considered here, only discrete-time samples of the agents' closed-loop trajectories $(\mathbf{x}(t_k), \dot{\mathbf{x}}(t_k), \mathbf{u}_1(t_k), \mathbf{u}_2(t_k))$ are available, while the objective components (Q_i, V_i, \mathbf{R}_i) are unknown. We assume measurements are collected at times $t_k = k\Delta t$, and $\dot{\mathbf{x}}(t_k)$ is obtained either from the known dynamics (1) or from filtered finite

differences. The observed behavior is assumed to approximately satisfy the HJB relations (4) and the feedback structure (5).

Problem statement. Given dynamics (1) and observed trajectories, infer probabilistic models of the unknown objective components (Q_i, V_i, \mathbf{R}_i) whose posterior realizations approximately satisfy the Hamilton–Jacobi–Bellman relations (4) together with the corresponding feedback conditions (5). The aim is to obtain predictive distributions over players' admissible equilibrium behavior across interactive settings.

To obtain a tractable inference procedure, we next introduce a feature-based parametrization of the objectives that makes the HJB relations linear in the decision parameters.

3. FEATURE-BASED INVERSE DIFFERENTIAL GAMES

We now introduce the feature-based parametrization used to represent the unknown objectives (V_i, Q_i, \mathbf{R}_i) . Let $\Omega \subset \mathbb{R}^{n_x}$ be a compact subset of the state space containing all observed trajectories. On Ω , stabilizing feedback laws yield value functions V_i that are locally Lipschitz and differentiable almost everywhere. Under standard regularity conditions, V_i belongs to a suitable Sobolev space on Ω , and classical approximation results (e.g., Weierstrass and universal approximation theorems (Abu-Khalaf and Lewis, 2005; Adams and Fournier, 2003)) ensure that both V_i and its gradient can be approximated arbitrarily well on Ω . Accurate approximation of ∇V_i is particularly important, as it enters the HJB relations directly and hence determines the Hamiltonian residuals used for inverse inference.

To obtain a tractable, linear-in-parameters representation of the unknown objectives, we approximate the value and state cost functions using differentiable feature maps

$$\phi_{V_i} : \Omega \rightarrow \mathbb{R}^{p_i}, \quad \phi_{Q_i} : \Omega \rightarrow \mathbb{R}^{s_i},$$

with typical choices including polynomial features, radial basis functions, or other standard universal approximators. The feature sets may incorporate task- or domain-specific structure (e.g., known symmetries or dominant state interactions) and are selected to provide smooth approximations compatible with the HJB relations. The control cost does not require approximation: since $\mathbf{u}_i^\top \mathbf{R}_i \mathbf{u}_i$ is quadratic in \mathbf{u}_i , it admits an exact linear parameterization through

$$\phi_{R_i}(\mathbf{u}_i) := \text{vec}(\mathbf{u}_i \mathbf{u}_i^\top) \in \mathbb{R}^{z_i}.$$

Under these representations, the objectives take the form

$$V_i(\mathbf{x}) = \mathbf{W}_{V_i}^\top \phi_{V_i}(\mathbf{x}) + \varepsilon_{V_i}(\mathbf{x}), \quad (6a)$$

$$Q_i(\mathbf{x}) = \mathbf{W}_{Q_i}^\top \phi_{Q_i}(\mathbf{x}) + \varepsilon_{Q_i}(\mathbf{x}), \quad (6b)$$

$$\mathbf{u}_i^\top \mathbf{R}_i \mathbf{u}_i = \mathbf{W}_{R_i}^\top \phi_{R_i}(\mathbf{u}_i), \quad (6c)$$

where terms ε_{V_i} and ε_{Q_i} capture the approximation error, which decreases for standard universal or increasing-order feature families as (p_i, s_i) grow. In contrast, the control cost is represented exactly, as $\mathbf{u}_i^\top \mathbf{R}_i \mathbf{u}_i$ is linear in the entries of \mathbf{R}_i . The parameters $\mathbf{W}_{V_i} \in \mathbb{R}^{p_i}$, $\mathbf{W}_{Q_i} \in \mathbb{R}^{s_i}$, and $\mathbf{W}_{R_i} \in \mathbb{R}^{z_i}$ encode the unknown objectives; recovering them is therefore equivalent to solving the inverse differential game. Observed trajectory samples yield data

through the HJB and feedback relations, and the aim is to infer posterior distributions over the weights such that

$$\mathcal{H}_i(\mathbf{x}, \mathbf{u}_1, \mathbf{u}_2; \mathbf{W}_{V_i}, \mathbf{W}_{Q_i}, \mathbf{W}_{R_i}) \approx 0$$

along the observed trajectories.

3.1 HJB conditions in feature space.

Substituting (6) into the stationary HJB equation (4) and using the dynamics (1) yields the linear-in-parameters condition

$$0 = \mathbf{W}_{Q_i}^\top \phi_{Q_i}(\mathbf{x}) + \mathbf{W}_{R_i}^\top \phi_{R_i}(\mathbf{u}_i) + \mathbf{W}_{V_i}^\top \nabla \phi_{V_i}(\mathbf{x}) \dot{\mathbf{x}} + \eta_i^{\text{HJB}}, \quad (7)$$

where η_i^{HJB} collects the approximation errors ε_{V_i} , ε_{Q_i} and their gradients. These terms are treated as residual noise in the regression model below.

Similarly, substituting into the feedback law (5) gives

$$\mathbf{u}_i = -\frac{1}{2} \mathbf{R}_i^{-1} \mathbf{g}_i(\mathbf{x})^\top \nabla \phi_{V_i}(\mathbf{x})^\top \mathbf{W}_{V_i} + \eta_i^{\text{fb}}, \quad (8)$$

where η_i^{fb} captures the corresponding approximation error.

Collecting all unknown coefficients in

$$\mathbf{W}_i = [\mathbf{W}_{V_i}^\top \ \mathbf{W}_{Q_i}^\top \ \mathbf{W}_{R_i}^\top]^\top,$$

the relations (7)–(8) yield linear constraints on \mathbf{W}_i up to residual noise terms. Since inverse differential-game objectives are identifiable only up to a positive scale factor (Self et al., 2021), we fix $R_{i,[11]}$ and remove this entry, yielding the reduced vector

$$\mathbf{W}_i^- = [\mathbf{W}_{V_i}^\top \ \mathbf{W}_{Q_i}^\top \ (\mathbf{W}_{R_i}^-)^\top]^\top.$$

Constant offsets in V_i do not affect the feedback law and are omitted, so \mathbf{W}_i^- represents one element of the equivalence class consistent with the observed behavior.

This leads to the regression model

$$\mathbf{y}_i = \Phi_i \mathbf{W}_i^- + \boldsymbol{\eta}_i, \quad (9)$$

where $\boldsymbol{\eta}_i$ collects residual terms arising from finite-dimensional approximation (6), numerical differentiation, and deviations from exact HJB optimality along the observed trajectories. The regressor and target follow directly from the HJB stationarity and feedback optimality conditions, with the regressor matrix given by

$$\Phi_i = \begin{bmatrix} (\nabla \phi_{V_i} \dot{\mathbf{x}})^\top & \phi_{Q_i}^\top & \phi_{R_i}^{-, \top} \\ \mathbf{g}_i^\top \nabla \phi_{V_i}^\top & \mathbf{0}_{m_i \times s_i} & \begin{bmatrix} \mathbf{0}_{1 \times (z_i-1)} \\ 2 \text{diag}(\mathbf{u}_{i,2:n_{u_i}}) \end{bmatrix} \end{bmatrix}, \quad (10)$$

where the bottom-right block reflects the gradient of $\mathbf{u}_i^\top \mathbf{R}_i \mathbf{u}_i$ with respect to the remaining entries of \mathbf{R}_i after removing the fixed element $R_{i,[11]}$. The regression target becomes

$$\mathbf{y}_i = \begin{bmatrix} -R_{i,[11]} u_{i,1}^2 \\ -2R_{i,[11]} u_{i,1} \\ \mathbf{0}_{(n_{u_i}-1) \times 1} \end{bmatrix}, \quad (11)$$

recalling that $R_{i,[11]}$ is fixed to resolve the scale ambiguity in the inverse HJB formulation.

The first row enforces the HJB stationarity condition (7), while the remaining rows encode the optimality conditions (8). The linear form (9) enables conjugate Bayesian updates for real-time, uncertainty-aware inference of the players' objectives.

4. BAYESIAN ONLINE ESTIMATION OF PLAYER OBJECTIVES

The linear relation (9) enables probabilistic inference over the reduced parameter vector \mathbf{W}_i^- . A Bayesian treatment is natural here: it allows prior structural information about the objectives to be incorporated and maintains an explicit representation of uncertainty, which propagates through the equilibrium feedback laws and induces predictive distributions over future inputs and state evolution.

At each sampling instant t_k , the available discrete-time measurements $(\mathbf{x}(t_k), \dot{\mathbf{x}}(t_k), \mathbf{u}_1(t_k), \mathbf{u}_2(t_k))$ are used to construct a data pair $(\Phi_i^{(k)}, \mathbf{y}_i^{(k)})$ via the feature-based representation of the HJB and feedback relations. Accounting for approximation error and deviations from exact optimality, each observation is modeled as

$$\mathbf{y}_i^{(k)} = \Phi_i^{(k)} \mathbf{W}_i^- + \boldsymbol{\eta}_i^{(k)}. \quad (12)$$

We adopt a Gaussian prior for \mathbf{W}_i^- ,

$$\mathbf{W}_i^- \sim \mathcal{N}(\mathbf{m}_{0,i}, \mathbf{S}_{0,i}), \quad (13)$$

which compactly encodes prior structure (e.g., expected scale or sparsity) and quantifies initial uncertainty. The disturbance term $\boldsymbol{\eta}_i^{(k)}$ is modeled as

$$\boldsymbol{\eta}_i^{(k)} \sim \mathcal{N}(\mathbf{0}, \boldsymbol{\Sigma}_i), \quad (14)$$

reflecting the aggregation of several independent error sources in the HJB residual—feature-approximation error, numerical differentiation of $\dot{\mathbf{x}}(t_k)$, and modeling mismatch—whose combined effect is well-approximated as Gaussian by standard central-limit arguments.

Under these linear–Gaussian assumptions, the posterior distribution of \mathbf{W}_i^- remains Gaussian and admits closed-form recursive updates, providing an efficient inference scheme suitable for online operation. The formulation here focuses on static objective parameters over a single interaction episode; extensions to time-varying objectives can be developed by placing a stochastic evolution model on \mathbf{W}_i^- .

4.1 Conjugate Bayesian Update

Let \mathcal{D}_k denote all data up to time t_k . Then

$$\mathbf{W}_i^- \mid \mathcal{D}_k \sim \mathcal{N}(\mathbf{m}_i^{(k)}, \mathbf{S}_i^{(k)}), \quad (15)$$

where $\mathbf{m}_i^{(k)}$ and $\mathbf{S}_i^{(k)}$ are the posterior mean and covariance.

Given a new sample $(\Phi_i^{(k+1)}, \mathbf{y}_i^{(k+1)})$, the updates are:

1) *Predicted output:*

$$\hat{\mathbf{y}}_i^{(k+1)} = \Phi_i^{(k+1)} \mathbf{m}_i^{(k)}. \quad (16)$$

2) *Predictive covariance:*

$$\mathbf{S}_{y,i} = \Phi_i^{(k+1)} \mathbf{S}_i^{(k)} \Phi_i^{(k+1)\top} + \boldsymbol{\Sigma}_i. \quad (17)$$

3) *Posterior gain:*

$$\mathbf{K}_i = \mathbf{S}_i^{(k)} \Phi_i^{(k+1)\top} \mathbf{S}_{y,i}^{-1}. \quad (18)$$

4) *Posterior mean:*

$$\mathbf{m}_i^{(k+1)} = \mathbf{m}_i^{(k)} + \mathbf{K}_i (\mathbf{y}_i^{(k+1)} - \hat{\mathbf{y}}_i^{(k+1)}). \quad (19)$$

5) *Posterior covariance:*

$$\mathbf{S}_i^{(k+1)} = (\mathbf{I} - \mathbf{K}_i \Phi_i^{(k+1)}) \mathbf{S}_i^{(k)} (\mathbf{I} - \mathbf{K}_i \Phi_i^{(k+1)})^\top + \mathbf{K}_i \Sigma_i \mathbf{K}_i^\top. \quad (20)$$

The update requires only the latest sample and the previous posterior; no history stack is maintained. The covariance $\mathbf{S}_i^{(k)}$ evolves in real time, reflecting how strongly the data support the inferred objective and highlighting inconsistencies with newly observed behavior through posterior shifts or increases in uncertainty.

4.2 Predictive Modeling and Monte Carlo Forecasting

Given the posterior $\mathcal{N}(\mathbf{m}_i^{(k)}, \mathbf{S}_i^{(k)})$ over the reduced parameter vector \mathbf{W}_i^- , the feedback law $\mu_i^*(\mathbf{x}; \mathbf{W}_i^-)$ in (8) induces a *stochastic policy model* for player i over a prediction rollout:

$$\mathbf{u}_i(t) = \mu_i^*(\mathbf{x}(t); \mathbf{W}_i^-), \quad \mathbf{W}_i^- \sim \mathcal{N}(\mathbf{m}_i^{(k)}, \mathbf{S}_i^{(k)}).$$

This stochastic policy is not executed by the agent; it reflects our belief, derived from data, about how the agent is likely to act under parameter uncertainty. Consequently, the induced closed-loop evolution is stochastic only through uncertainty in \mathbf{W}_i^- . For any horizon $T > 0$, the resulting distribution over trajectories is given by the pushforward measure

$$\mathcal{P}_{\mathbf{x}(\cdot)} = \Gamma_\# \left(\mathcal{N}(\mathbf{m}_i^{(k)}, \mathbf{S}_i^{(k)}) \right),$$

where Γ maps a parameter realization to its closed-loop trajectory on $[0, T]$.

Since this distribution is analytically intractable, we approximate it via Monte Carlo simulation. For each rollout $s = 1, \dots, N_{mc}$, we sample \mathbf{W}_i^{-s} from the posterior, generate the corresponding stochastic policy model, and simulate the closed-loop dynamics to obtain trajectories $\mathbf{x}^{(s)}(t)$ and $\mathbf{u}_i^{(s)}(t)$. We use the Monte Carlo rollouts to construct a *forecast envelope* for the predicted closed-loop evolution. For $t = 0 : T$ and state dimension n_x , we introduce componentwise bounds

$$\mathcal{X}_t(\theta) = \{\mathbf{x} \in \mathbb{R}^{n_x} : x_{t,j} \leq \bar{x}_{t,j}, j = 1:n_x\}, \quad (21)$$

parameterized by $\theta = \{\underline{x}_{t,j}, \bar{x}_{t,j}\}_{t=0:T, j=1:n_x} \in \mathbb{R}^d$, where $d = 2(T+1)n_x$. We focus on state envelopes for clarity, although the same construction applies to the predicted input sequence $\mathbf{u}_i(t)$ obtained from the Monte Carlo rollouts.

Theorem 1 (Reliability of the Forecast Envelope). *Let θ^* denote an envelope parameter obtained from the Monte Carlo trajectories $\mathbf{x}^{(s)}(t) = \Gamma(\mathbf{W}_i^{-s})(t)$, $s = 1 : N_{mc}$, $t = 0 : T$. For any $\varepsilon, \beta \in (0, 1)$, if the number of samples N_{mc} satisfies*

$$\sum_{i=0}^{d-1} \binom{N_{mc}}{i} \varepsilon^i (1-\varepsilon)^{N_{mc}-i} \leq \beta, \quad (22)$$

then

$$\mathbb{P}(V(\theta^*) \leq \varepsilon) \geq 1 - \beta,$$

where $V(\theta) = \mathbb{P}_{\mathbf{W}_i^-} \{\exists t : \Gamma(\mathbf{W}_i^-)(t) \notin \mathcal{X}_t(\theta)\}$, and the probability is with respect to the draw of the N_{mc} posterior samples.

Proof. Each rollout is generated by independently sampling $\mathbf{W}_i^{-s} \sim \mathcal{N}(\mathbf{m}_i^{(k)}, \mathbf{S}_i^{(k)})$ and propagating it through the closed-loop map Γ . Thus the constraints $\mathbf{x}^{(s)}(t) \in \mathcal{X}_t(\theta)$ correspond to i.i.d. scenario constraints associated with the uncertainty \mathbf{W}_i^- .

A forecast envelope θ^* can be obtained by solving the convex scenario program

$$\theta^* \in \arg \min_{\theta} \left\{ \sum_{t=0}^T \sum_{j=1}^{n_x} (\bar{x}_{t,j} - \underline{x}_{t,j}) \right\} \text{ s.t. } \mathbf{x}^{(s)}(t) \in \mathcal{X}_t(\theta), \quad \forall s = 1:N_{mc}, t = 0 : T.$$

The decision variable enters these constraints only through affine inequalities, and the objective is linear; thus the program is convex. By the scenario approach for convex programs (Campi and Garatti, 2008), any such solution θ^* satisfies

$$\mathbb{P}(V(\theta^*) > \varepsilon) \leq \sum_{i=0}^{d-1} \binom{N_{mc}}{i} \varepsilon^i (1-\varepsilon)^{N_{mc}-i},$$

and condition (22) ensures this probability is at most β . \square

Theorem 1 establishes that the forecast envelope $\{\mathcal{X}_t^*\}_{t=0}^T$, constructed from the Monte Carlo ensemble, enjoys a reliability guarantee with respect to the posterior over \mathbf{W}_i^- . With confidence at least $1 - \beta$ (over the randomness of the training rollouts), the probability that a new trajectory sampled from the posterior exits the envelope over the prediction horizon is at most ε . The binomial condition (22) characterizes the trade-off between ensemble size, violation level, and confidence: given (ε, β) , the required number of Monte Carlo rollouts N_{mc} is the smallest integer satisfying (22); conversely, for a fixed ensemble size N_{mc} and a confidence level $1 - \beta$, the certified violation probability $\bar{\varepsilon}$ is the smallest value of ε for which (22) holds. These guarantees are non-asymptotic and depend only on the envelope parameterization dimension d and the number of posterior samples, in accordance with standard results from the scenario approach (Campi and Garatti, 2008). The Monte Carlo ensemble and the resulting forecast envelope provide empirical moments, nonparametric credible regions, and a scenario-certified bound on predicted states and inputs, enabling uncertainty-aware downstream tasks such as probabilistic constraint checking, risk assessment, or anticipating opponent behavior.

5. SIMULATIONS AND RESULTS

5.1 Linear-Quadratic (LQ) Inverse Game

We first evaluate the proposed Bayesian inverse-game method on a linear-quadratic (LQ) differential game adapted from (Inga et al., 2021).¹ In this setting, closed-form Nash equilibria can be computed efficiently (e.g., via the Lyapunov-iteration algorithm of (Li and Gajic, 1995)), enabling direct comparison between the inferred parameters and ground truth. The system error dynamics are

$$\dot{\mathbf{x}}(t) = A\mathbf{x}(t) + B_1\mathbf{u}_1(t) + B_2\mathbf{u}_2(t), \quad (23)$$

¹ Code for the algorithm and simulations is available at <https://github.com/TUM-ITR/bayesian-agent-behavior>.

with matrices

$$A = \begin{pmatrix} 0 & 1 & -1 & 0 \\ 1 & 0 & 2 & 1 \\ 0 & -2 & 0 & 1 \\ 0 & 1 & 0 & -1 \end{pmatrix}, \quad B_1 = \frac{1}{2} \begin{pmatrix} 0 & 1 \\ 0 & 0 \\ 0 & 0 \\ 1 & 0 \end{pmatrix}, \quad B_2 = \frac{1}{2} \begin{pmatrix} 0 & 0 \\ 0 & 1 \\ 1 & 0 \\ 0 & 0 \end{pmatrix}.$$

The nominal (mean) cost matrices are

$$Q_{1,\text{mean}} = \text{diag}(1, 2/5, 3, 1), \quad R_{1,\text{mean}} = \text{diag}(1, 1), \\ Q_{2,\text{mean}} = \text{diag}(1, 2/3, 1, 2), \quad R_{2,\text{mean}} = \text{diag}(1, 0.5).$$

As in standard inverse-LQ formulations, the intrinsic scale ambiguity is removed by treating $R_{i,[11]}$ as known. The remaining diagonal entries of Q_i and R_i are sampled independently from Gaussians centered at their nominal values, with variances

$$\text{Var}(Q_1) = \text{diag}(1, 0.16, 9, 1), \quad \text{Var}(R_{1,[22]}) = 1, \\ \text{Var}(Q_2) = \text{diag}(1, 4/9, 1, 4), \quad \text{Var}(R_{2,[22]}) = \frac{1}{4}.$$

Thus, for all non-fixed entries,

$$Q_{i,[jj]} \sim \mathcal{N}(Q_{i,[jj],\text{mean}}, \text{Var}(Q_{i,jj})), \quad (24a)$$

$$R_{i,[22]} \sim \mathcal{N}(R_{i,[22],\text{mean}}, \text{Var}(R_{i,22})). \quad (24b)$$

The prior mean $\mathbf{m}_{i,0}$ is constructed from the nominal cost matrices and the associated value-function solutions $V_i(\mathbf{x}) = \mathbf{x}^\top P_i \mathbf{x}$. The corresponding quadratic feature map is

$$\phi_{V_i}(\mathbf{x}) = [x_1^2, x_1 x_2, \dots, x_3 x_4, x_4^2]^\top.$$

In the LQ setting, the known quadratic structure of the value function allows for a reliable estimation of parameter variability. A Monte Carlo procedure using 200 samples drawn from (24) is used to compute the associated value functions and obtain a sample-based characterization of feature-parameter variability. Together with the priors in (24), this yields the prior $(\mathbf{m}_{i,0}, \mathbf{S}_{i,0})$.

We then run the online Bayesian inverse-game algorithm on data generated from an LQ game initialized at

$$\mathbf{x}_0 = [3, -4, 2, 1.5]^\top.$$

To capture representative closed-loop behavior in a range of task-relevant configurations, the system is successively regulated toward three intermediate targets:

$$\mathbf{x}_1 = \mathbf{0}^\top, \quad \mathbf{x}_2 = [1, -2, 2, 1]^\top, \quad \mathbf{x}_3 = [-2, 1, 3, -2]^\top,$$

with data sampled at $\Delta t = 0.01$ s.

Figure 1 shows the Bayesian prediction of the game parameters for Player 1. The posterior means converge rapidly to the true values, while the shaded 2σ region shrinks as more data are incorporated, indicating growing confidence in the inferred objective. Parameters that are more strongly excited by the trajectory tighten earlier, illustrating the data-adaptive nature of the online estimator.

Next, we demonstrate how the algorithm enables probabilistic predictions of adversarial behavior. We assume the role of Player 2 and estimate Player 1's objective using only the first 30 data samples, representing an early-phase interaction where prior knowledge is limited. The resulting posterior is then used to predict Player 1's future inputs and the corresponding closed-loop state evolution. All prediction rollouts are initialized from the same state \mathbf{x}_0 as in the parameter-identification evaluation. To visualize typical predicted behavior, we draw $N_{\text{mc}} = 10000$ samples

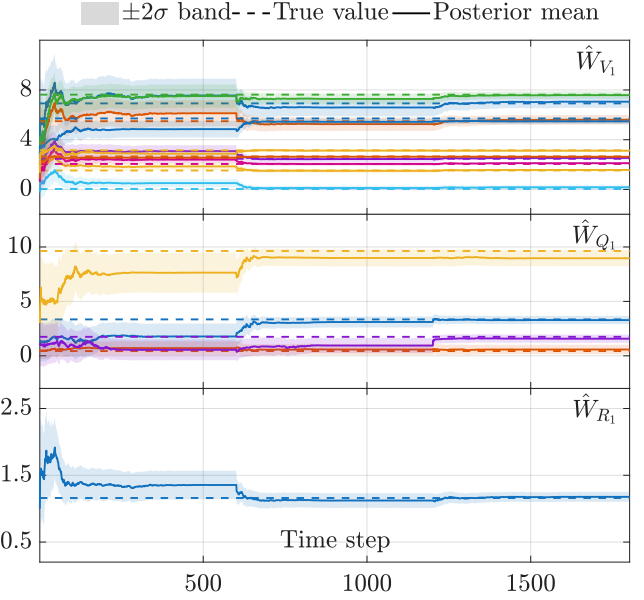


Fig. 1. Convergence of the inferred game parameters for Player 1. The dashed lines denote the true values, solid lines show the posterior means, and the shaded regions represent the $\pm 2\sigma$ uncertainty. The three panels correspond to value-function weights, state-cost weights, and the unknown input-cost weight.

from the posterior and propagate them through the dynamics. Figure 2 shows the predicted inputs for both control channels: the posterior mean closely follows the true input signals, while the 95% credible regions—computed as pointwise empirical quantiles—expand in portions of the trajectory where Player 1's behavior is harder to predict. An analogous plot for the state evolution is provided in Figure 3. In both figures, we additionally overlay the scenario-certified forecast envelopes (dashed lines), allowing a direct comparison between empirical credible regions and guaranteed bounds.

It is worth noting that visually stable credible regions typically require only a modest number of Monte Carlo samples, whereas scenario-theoretic guarantees are more demanding. In this experiment, the prediction horizon spans $T = 6$ s with a sampling time of $\Delta t = 0.1$ s, resulting in a long sequence of envelope parameters; obtaining non-trivial violation bounds therefore necessitates a sufficiently large number of rollout samples. Using the same N_{mc} Monte Carlo rollouts, we construct the forecast envelope introduced in Section 4.2. Applying Theorem 1 with confidence level $1 - \beta = 0.99$ yields a certified violation probability of $\varepsilon = 0.0531$. That is, with 99% confidence (over the randomness of the posterior sampling), a trajectory drawn from the posterior exits the forecast envelope with probability at most 5.31%.

In summary, the 95% credible regions describe the typical spread of posterior predictions at each time step, while the scenario-certified forecast envelope provides a rigorous, distribution-free guarantee on the entire predicted trajectory. Both are derived from the same Monte Carlo ensemble and together offer a comprehensive characterization of uncertainty in Player 1's predicted behavior.

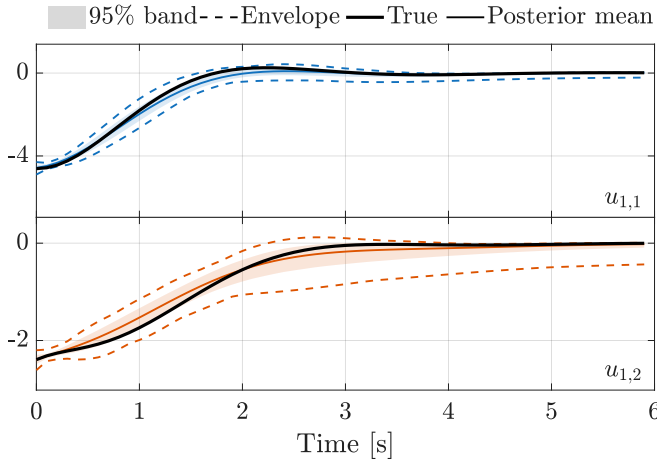


Fig. 2. Predicted inputs of Player 1 under uncertain cost estimation. True inputs (thick solid), posterior means (solid), 95% credible regions (shaded), and scenario-certified forecast envelopes (dashed, colored) are shown for both control channels (blue and orange).

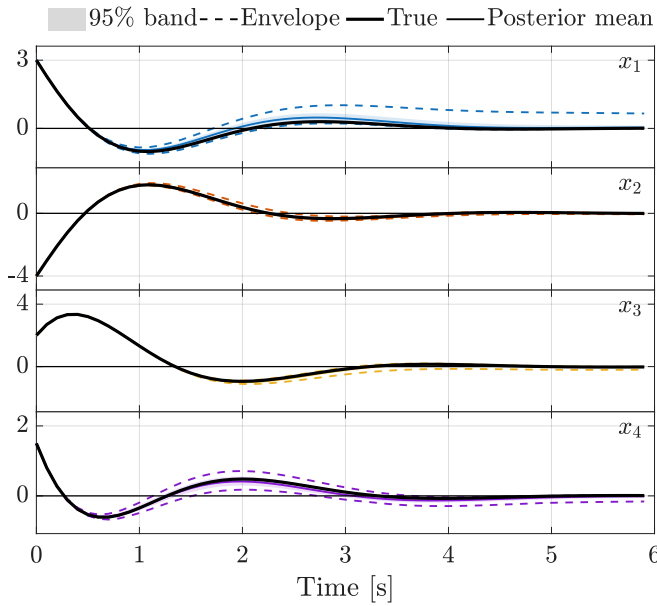


Fig. 3. Predicted state trajectories under uncertainty in Player 1's behavior. True trajectories (thick solid), posterior means (solid), 95% credible regions (shaded), and scenario-certified forecast envelopes (dashed, colored) are shown for all state components.

5.2 Nonlinear Shared-Control Example

We next consider a nonlinear one-dimensional differential game that reflects characteristic features of shared-control scenarios in HRI. Unlike the LQ example, the interaction dynamics are state-dependent and non-affine, yielding configuration-dependent and highly nonuniform influence of the two players. The drift and input channels are

$$f(x) = \frac{-0.5x - 0.3x^3}{b(x)}, \quad (25a)$$

$$g_1(x) = \frac{1.2 + 0.8 \sin(1.5x)}{b(x)}, \quad (25b)$$

$$g_2(x) = \frac{1.0 - 0.7 \sin(1.5x + \pi/3)}{b(x)}, \quad (25c)$$

where

$$b(x) = b_0(1 + \beta x^2), \quad b_0 = 2.0, \beta = 0.3,$$

models a state-dependent “inertia” term.

The oscillatory structure of (g_1, g_2) creates alternating regions in which either the human or the robot dominates the effective control authority. Such patterns are representative of physical shared-control settings where task geometry or interaction constraints induce configuration-dependent responsiveness. The resulting game is more challenging than the LQ case because the players’ influence varies across the state space, and the HJB relations are nonlinear even after fixing the running costs.

Each player uses a quadratic running cost

$$\ell_i(x, u_i) = Q_i x^2 + R_i u_i^2, \quad R_1 = R_2 = 1, \quad (26)$$

with unknown positive parameters Q_i . To generate realistic ground truth while capturing prior variability, each Q_i is sampled from a Gaussian distribution with means

$$Q_{1,\text{mean}} = 1.0, \quad Q_{2,\text{mean}} = 0.3. \quad (27)$$

and variances

$$\text{Var}(Q_1) = 0.5 \quad \text{Var}(Q_2) = 0.18. \quad (28)$$

For these sampled costs, the coupled nonlinear HJB equations associated with (25) and (26) are solved numerically on a compact domain using a Legendre basis of order 10. The resulting value functions $V_i^*(x)$ are used both to generate expert trajectories and to benchmark the Bayesian inverse-game identification.

We simulate two regulation tasks, starting from $x_0 = 4$ and $x_1 = -4$, over an 8s horizon, collecting data at each time step. The Bayesian inverse-game algorithm is then run online along the resulting trajectory. Figure 4 shows the estimated value functions after 500 updates ($t = 5$ s). The posterior means closely match the true value functions on the portions of the state space visited by the system, while the uncertainty remains higher in regions that receive little or no data (e.g., $x \leq -4$ or $x \geq 4$). This illustrates the estimator’s ability to recover nonlinear objective structure where information is available and to reflect appropriate uncertainty elsewhere.

6. CONCLUSION

We introduced an online Bayesian framework for inverse differential games based on Hamilton–Jacobi–Bellman relations. By combining feature-based HJB residuals with Gaussian priors, the method enables uncertainty-aware inference, informative early predictions, and recursive updates without history stacks. The framework applies to linear and nonlinear dynamics and supports general value-function representations, making it suitable for adaptive, risk-aware multi-agent interaction. Future work will explore time-varying objectives, richer nonparametric models, and validation in human–robot interaction scenarios.

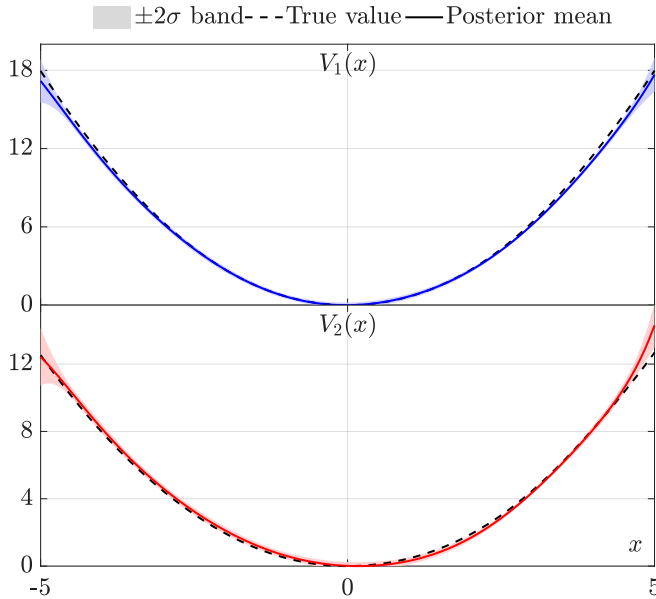


Fig. 4. Estimated value functions for game (25) after 500 updates ($t = 5$ s). True value functions (dashed), posterior means (solid), and corresponding confidence regions (shaded). Blue: Player 1; Red: Player 2.

DECLARATION OF GENERATIVE AI AND AI-ASSISTED TECHNOLOGIES IN THE WRITING PROCESS

During the preparation of this work, the authors used OpenAI's ChatGPT to assist with text revision and improvement of clarity. After using this tool, the authors reviewed and edited the content as needed and take full responsibility for the final version of the manuscript.

REFERENCES

Abu-Khalaf, M. and Lewis, F.L. (2005). Nearly optimal control laws for nonlinear systems with saturating actuators using a neural network hjb approach. *Automatica*, 41(5), 779–791.

Adams, R.A. and Fournier, J.J. (2003). *Sobolev spaces*, volume 140. Elsevier.

Arora, S. and Doshi, P. (2021). A survey of inverse reinforcement learning: Challenges, methods and progress. *Artificial Intelligence*, 297, 103500.

Basar, T. and Olsder, G.J. (1999). *Dynamic noncooperative game theory*. 2nd ed. (*Classics in applied mathematics* 23). Society for Industrial and Applied Mathematics, United States.

Bianchin, F., Lefringhausen, R., Gaetan, E., Tesfazgi, S., and Hirche, S. (2025). A set-theoretic robust control approach for linear quadratic games with unknown counterparts.

Campi, M.C. and Garatti, S. (2008). The exact feasibility of randomized solutions of uncertain convex programs. *SIAM Journal on Optimization*, 19(3), 1211–1230.

Engwerda, J. (2005). *LQ Dynamic Optimization and Differential Games*. John Wiley & Sons.

Inga, J., Bischoff, E., Molloy, T.L., Flad, M., and Hohmann, S. (2019). Solution sets for inverse non-cooperative linear-quadratic differential games. *IEEE Control Systems Letters*, 3(4), 871–876.

Inga, J., Creutz, A., and Hohmann, S. (2021). Online inverse linear-quadratic differential games applied to human behavior identification in shared control. In *2021 European Control Conference (ECC)*, 353–360.

Isaacs, R. (1965). *Differential Games: A Mathematical Theory with Applications to Warfare and Pursuit, Control and Optimization*. Dover books on mathematics. Wiley.

Li, T.Y. and Gajic, Z. (1995). Lyapunov iterations for solving coupled algebraic riccati equations of nash differential games and algebraic riccati equations of zero-sum games. In *New Trends in Dynamic Games and Applications*, 333–351. Springer.

Li, Y., Tee, K.P., Yan, R., Chan, W.L., and Wu, Y. (2016). A framework of human–robot coordination based on game theory and policy iteration. *IEEE Transactions on Robotics*, 32(6), 1408–1418.

Molloy, T.L., Charaja, J.I., Hohmann, S., and Perez, T. (2022). *Inverse optimal control and inverse noncooperative dynamic game theory*. Springer.

Musić, S. and Hirche, S. (2020). Haptic shared control for human–robot collaboration: A game-theoretical approach. *IFAC-PapersOnLine*, 53(2), 10216–10222. 21st IFAC World Congress.

Na, X. and Cole, D.J. (2019). Modelling of a human driver's interaction with vehicle automated steering using cooperative game theory. *IEEE/CAA Journal of Automatica Sinica*, 6(JAS-2019-0028), 1095.

Self, R., Coleman, K., Bai, H., and Kamalapurkar, R. (2021). Online observer-based inverse reinforcement learning. *IEEE Control Systems Letters*, 5(6), 1922–27.

Self, R., Harlan, M., and Kamalapurkar, R. (2018). Online inverse reinforcement learning for nonlinear systems. *2019 IEEE Conference on Control Technology and Applications (CCTA)*, 296–301.

Vamvoudakis, K.G. and Lewis, F.L. (2011). Multi-player non-zero-sum games: Online adaptive learning solution of coupled hamilton–jacobi equations. *Automatica*, 47(8), 1556–1569.